Modulation Transfer Function in Optical and Electro-Optical Systems

Second Edition

Glenn D. Boreman

Tutorial Texts in Optical Engineering
Volume TT121

SPIE PRESS
Bellingham, Washington USA

Library of Congress Cataloging-in-Publication Data

Names: Boreman, G. D. (Glenn D.), author.
Title: Modulation transfer function in optical and electro-optical systems / Glenn D. Boreman.
Description: Second edition. | Bellingham, Washington : SPIE Press, [2021] | Series: Tutorial texts in optical engineering ; Volume TT121 | Includes bibliographical references and index.
Identifiers: LCCN 2020043215 (print) | LCCN 2020043216 (ebook) | ISBN 9781510639379 (paperback) | ISBN 9781510639386 (pdf)
Subjects: LCSH: Optics. | Electrooptical devices. | Modulation theory.
Classification: LCC TA1520 .B67 2021 (print) | LCC TA1520 (ebook) | DDC 621.36--dc23
LC record available at https://lccn.loc.gov/2020043215
LC ebook record available at https://lccn.loc.gov/2020043216

Published by

SPIE
P.O. Box 10
Bellingham, Washington 98227-0010 USA
Phone: +1 360.676.3290
Fax: +1 360.647.1445
Email: books@spie.org
Web: http://spie.org

Printed in the United States of America.
First printing.
For updates to this book, visit http://spie.org and type “TT121” in the search field.

SPIE.

Contents

Preface to the Second Edition

It had been 19 years since the first edition of this book, when the extended quarantine period of 2020 afforded me the rare opportunity of quiet time away from my usual administrative and research activities. I have significantly expanded the treatment of several topics, including bar-target measurements, noise-target measurements, effects of aberrations, and slant-edge measurements. I have been gratified by the recent industrial and government-lab interest in the speckle techniques, which, after all, comprised a good portion of my dissertation at University of Arizona some 36 years ago. All other topics in the book were reviewed and updated, with recent references added. I have kept my original emphasis on practical issues and measurement techniques.

I acknowledge with pleasure discussions about MTF with colleagues and their students here at UNC Charlotte, among whom are Profs. Angela Allen, Chris Evans, and Thomas Suleski. During the writing process, I appreciated receiving daily encouragement by telephone from Dot Graudons, daily encouragement via WhatsApp from Prof. Mike Sundheimer of the Universidade Federal Rural de Pernambuco in Recife Brazil, and weekly encouragement via Zoom from Skye Engel. I am grateful for the permissions granted for reproductions of some of the figures from their original sources, to the two anonymous reviewers for their insightful and helpful comments, and to Dara Burrows of SPIE Press for her expert copyediting.

Last but surely not least, I want to thank Maggie Boreman – my wife of 30 years, my main encourager, and technical editor. You have graciously taken time from your equestrian pleasures to struggle, once again, with turning my writing into something approaching standard English. Thanks.

Glenn D. Boreman
Emerald Rose Farm
23 November 2020

Chapter 1
MTF in Optical Systems

Linear-systems theory provides a powerful set of tools with which we can analyze optical and electro-optical systems. The spatial impulse response of the system is Fourier transformed to yield the spatial-frequency optical transfer function. These two viewpoints are equivalent ways to describe an object—as a collection of points or as a summation of spatial frequencies. Simply expressing the notion of image quality in the frequency domain does not by itself generate any new information. However, the conceptual change in viewpoint—instead of a spot size, we now consider a frequency response—provides additional insight into the behavior of an imaging system, particularly in the common situation where several subsystems are combined. We can multiply the individual transfer function of each subsystem to give the overall transfer function. This procedure is easier than the repeated convolutions that would be required for a spatial-domain analysis, and allows immediate visualization of the performance limitations of the aggregate system in terms of the performance of each of the subsystems. We can see where the limitations of performance arise and which crucial components must be improved to yield better overall image quality. We directly see the effects of diffraction and aberrations at various spatial frequencies.

In Chapter 1 we develop the transfer-function concept and apply it to classical optical systems—imaging systems alone without detectors or electronics. We will first define terms and then discuss image-quality issues.

1.1 Impulse Response

The impulse response $h(x,y)$ is the smallest image detail that an optical system can form and is called the point-spread function (PSF). It is the blur spot in the image plane when a point source is the object of an imaging system. The finite width of the impulse response is a result of the combination of diffraction and aberration effects. We interpret $h(x,y)$ as an irradiance (W/cm^2) distribution that is a function of the image-plane position. Modeling

the imaging process as a convolution operation (denoted by *), we express the image irradiance distribution $g(x,y)$ as the ideal image $f(x,y)$ convolved with the impulse response $h(x,y)$:

$$g(x,y) = f(x,y) * h(x,y). \tag{1.1}$$

The ideal image $f(x,y)$ is the irradiance distribution that would exist in the image plane (taking into account the system magnification) if the system had perfect image quality, in other words, a delta-function impulse response. The ideal image is thus a magnified version of the input-object irradiance, with all detail preserved. For conceptual discussions, we typically assume that the imaging system has unit magnification, so for the ideal image we can directly take $f(x,y)$ as the object irradiance distribution, albeit as a function of image-plane coordinates x and y. We can see from Eq. (1.1) that if $h(x,y) = \delta(x,y)$, the image would be a perfect replica of the object. A perfect optical system is capable of forming a point image of a point object. However, because of the blurring effects of diffraction and aberrations, a real imaging system has an impulse response that is not a point. For any real system, $h(x,y)$ has a finite spatial extent. It is within this context that $h(x,y)$ is referred to as the point-spread function (PSF)—the image-plane irradiance corresponding to a point source input. The narrower the PSF, the less blurring occurs in the image-forming process. A more compact impulse response indicates better image quality.

As Fig. 1.1 illustrates, we represent mathematically a point object as a delta function at location (x',y') in object-plane coordinates:

$$f(x_{\text{obj}}, y_{\text{obj}}) = \delta(x' - x_{\text{obj}}, y' - y_{\text{obj}}). \tag{1.2}$$

Assuming that the system has unit magnification, the ideal image is a delta function located at (x',y') in image-plane coordinates:

$$g(x,y) = \delta(x' - x, y' - y). \tag{1.3}$$

In a real imaging system, the response to the delta-function object of Eq. (1.2) is the impulse response $g(x,y) = h(x' - x, y' - y)$, centered at $x = x'$

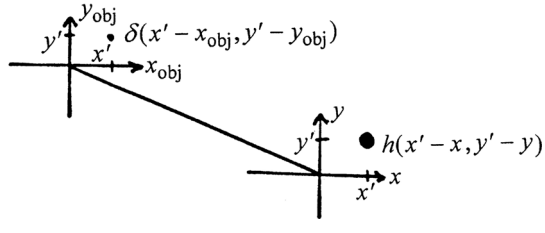

Figure 1.1 A delta function in the object plane is mapped to a blur function, the impulse response, in the image plane.

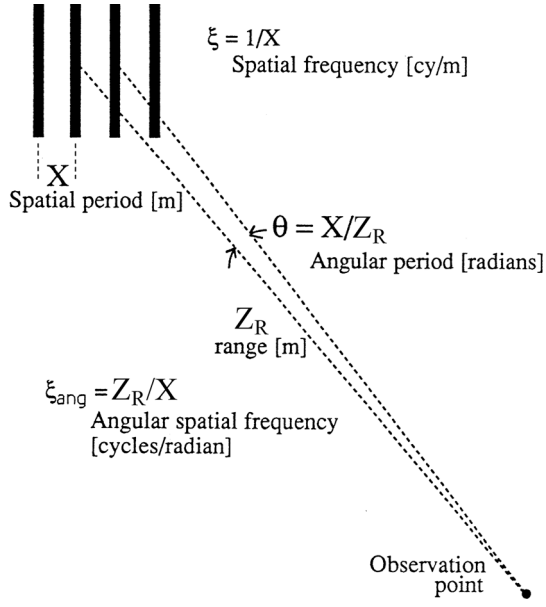

Figure 1.6 Angular spatial frequency.

1.3 Transfer Function

Equation (1.1) describes the loss of detail inherent in the imaging process as the convolution of the ideal image function with the impulse response. The convolution theorem[4] states that a convolution in the spatial domain is a multiplication in the frequency domain. Taking the Fourier transform (denoted as $\mathcal{F}$) of both sides of Eq. (1.1) yields

$$\mathcal{F}\{g(x,y)\} = \mathcal{F}\{f(x,y) * h(x,y)\} \tag{1.6}$$

and

$$G(\xi,\eta) = F(\xi,\eta) \times H(\xi,\eta), \tag{1.7}$$

where uppercase functions denote the Fourier transforms of the corresponding lowercase functions: F denotes the object spectrum, G denotes the image spectrum, and H denotes the spectrum of the impulse response. $H(\xi,\eta)$ is the transfer function; it relates the object and image spectra multiplicatively. The Fourier transform changes the irradiance waveform from a spatial-position function to the spatial-frequency domain but generates no new information. The appeal of the frequency-domain viewpoint is that the multiplication of Eq. (1.7) is easier to perform and visualize than the convolution of Eq. (1.1). This convenience is most apparent in the analysis of imaging systems consisting of several subsystems, each with its own impulse response.

dramatic artifact is that the image now has five peaks instead of the four seen in the previous cases.

1.4 MTF and Resolution

Resolution is a quantity without a standardized definition. Figure 1.19 illustrates the image-irradiance-*vs*-position plots in the spatial domain, showing a particular separation distance for which images of two points are said to be resolved. A variety of criteria exist for such determination, based on the magnitude of the dip in irradiance between the point images. Resolution can be defined in image-plane distance or in object-space angular measure.

In addition to these definitions, resolution can be specified in the spatial-frequency domain as the frequency at which the MTF falls below a particular threshold. A typical value used in practice is 10%, but the required MTF threshold depends on the application. A threshold MTF and hence limiting resolution (Fig. 1.20) can be defined in terms of the noise-equivalent modulation (NEM), which is how much modulation depth is needed to give a unit signal-to-noise ratio, as a function of spatial frequency. We will

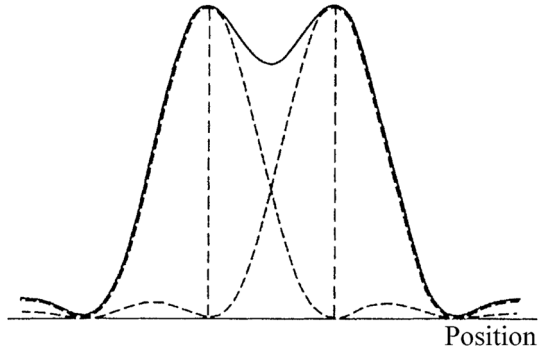

Figure 1.19 Resolution can be defined in the spatial domain.

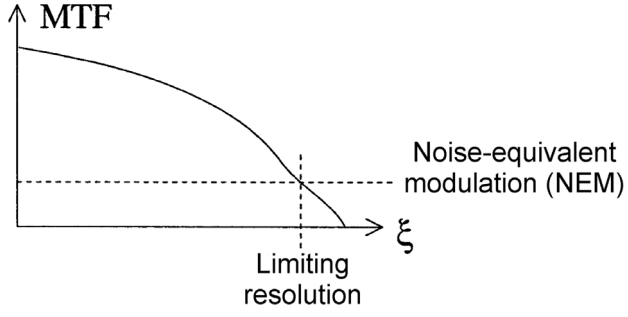

Figure 1.20 Resolution can be defined in the spatial-frequency domain.

A large Strehl ratio implies a large area under the MTF curve and high irradiance at the image location. Aberration effects such as those seen in Fig. 1.35 can be interpreted directly as the decrease in volume (area) under the MTF curve.

1.6.2 Effect of defocus on MTF

In Fig. 1.36 we compare a diffraction-limited OTF to that for systems with increasing amounts of defocus. The amount of defocus is expressed in terms of optical path difference (OPD), which is the wavefront error at the edge of the aperture in units of λ. In all cases, the diffraction-limited curve is the upper limit to the OTF. For small amounts of defocus, the OTF curve is pulled down only slightly. For additional defocus, a significant narrowing of the transfer function occurs. For a severely defocused system, we observe the phase-reversal phenomenon that we saw in the defocused image of the radial bar target of Fig. 1.14.

We can visualize the relationship between Strehl ratio and MTF by comparing the PSFs and MTFs for the diffraction-limited and λ/4-of-defocus conditions. For λ/4 of defocus, the transfer function is purely real, so OTF = MTF. From Fig. 1.37, we see that the defocus moves about 20% of the power from the center of the impulse response into the ring structure. The on-axis value of the impulse response is reduced, with a corresponding reduction in the area under the MTF curve.

1.6.3 Effects of other aberrations on MTF

To further visualize the effects of aberrations on MTF, let us compare the PSF and MTF for different amounts of wavefront error (WFE). The graphs on pages 31 to 33 show the PSFs (both as irradiance as a function of position and as a gray-level irradiance distribution), along with corresponding MTF plots.

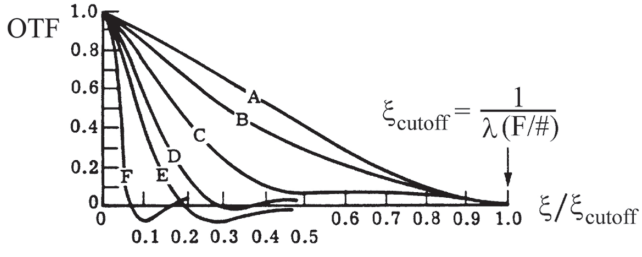

A:	focused: OPD = 0	D:	defocus: OPD = 3λ/4
B:	defocus: OPD = λ/4	E:	defocus: OPD = λ
C:	defocus: OPD = λ/2	F:	defocus: OPD = 5λ/4

Figure 1.36 Effect of defocus on the OTF of a diffraction-limited circular-aperture system (adapted from Ref. 13).

Chapter 2
MTF in Electro-optical Systems

In Chapter 1 we applied a transfer-function-based analysis to describe image quality in classical optical systems, that is, systems with optical components only. In this chapter we will examine the MTF of electro-optical systems, that is, systems that use a combination of optics, scanners, detectors, electronics, signal processors, and displays. To apply MTF concepts in the analysis of electro-optical systems, we must generalize our assumptions of linearity and shift invariance. Noise is inherent in any system with electronics. Linearity is not strictly valid for systems that have an additive noise level because image waveforms must be of sufficient irradiance to overcome the noise before they can be considered to add linearly. The classical MTF theory presented in Chapter 1 does not account for the effects of noise. We will demonstrate how to broaden the MTF concept to include this issue. Electro-optical systems typically include detectors or detector arrays for which the size of the detectors and the spatial sampling interval are both finite. Because of the shift-variant nature of the impulse response for sampled-data systems, we will develop the concept of an average impulse response obtained over a statistical ensemble of source positions to preserve the convenience of a transfer-function analysis. We will also develop an expression for the MTF impact of irradiance averaging over the finite sensor size. With these modifications, we can apply a transfer-function approach to a wider range of situations.

2.1 Detector Footprint MTF

We often think about the object as being imaged onto the detectors, but it is also useful to consider where the detectors are imaged. The footprint of a particular detector, called the instantaneous field of view (IFOV), is the geometrical projection of that detector into object space. We consider a scanned imaging system in Fig. 2.1 and a staring focal-plane-array (FPA) imaging system in Fig. 2.2. In each case, the flux falling onto an individual detector produces a single output. Inherent in the finite size of the detector elements is some spatial averaging of the image irradiance. For the

$$\mathrm{MTF}_{\mathrm{footprint}}(\xi,\eta) = \left| \frac{\sin(\pi\xi w_x)}{\pi\xi w_x} \right| \left| \frac{\sin(\pi\eta w_y)}{\pi\eta w_y} \right|. \tag{2.5}$$

The impulse response in Eq. (2.3) is separable, that is, $h_{\mathrm{footprint}}(x,y)$ is simply a function of x multiplied by a function of y. The simplicity of the separable case is that both $h(x,y)$ and $H(\xi,\eta)$ are products of two one-dimensional functions, with the x and y dependences completely separated. Occasionally, a situation arises in which the detector responsivity function is not separable.[2,3] In that case, we can no longer write the MTF as the product of two one-dimensional MTFs, as seen in Fig. 2.5. The MTF along the ξ and η spatial frequency directions is affected by both x and y profiles of the detector footprint. For example, the MTF along the ξ direction is not simply the Fourier transform of the x profile of the footprint but is

$$\mathrm{MTF}_{\mathrm{footprint}}(\xi, 0) = |H_{\mathrm{footprint}}(\xi, \eta = 0)| \neq |\mathcal{F}\{h_{\mathrm{footprint}}(x, y = 0)\}|. \tag{2.6}$$

Finding MTF in these situations requires a two-dimensional Fourier transform of the detector footprint. The transfer function can then be evaluated along the ξ or η axis, or along any other desired direction.

2.2 Sampling

Sampling is a necessary part of the data-acquisition process in any electro-optical system. We will sample at spatial intervals $\Delta x \equiv x_{\mathrm{samp}}$. The spatial sampling rate is determined by the location of the detectors in a focal-plane

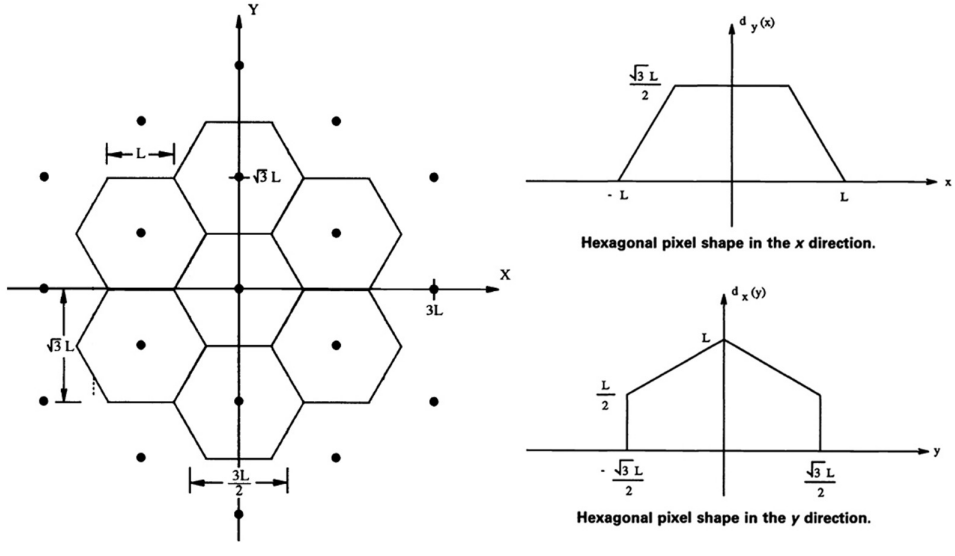

Figure 2.5 Example of a nonseparable detector footprint (adapted from Ref. 3).

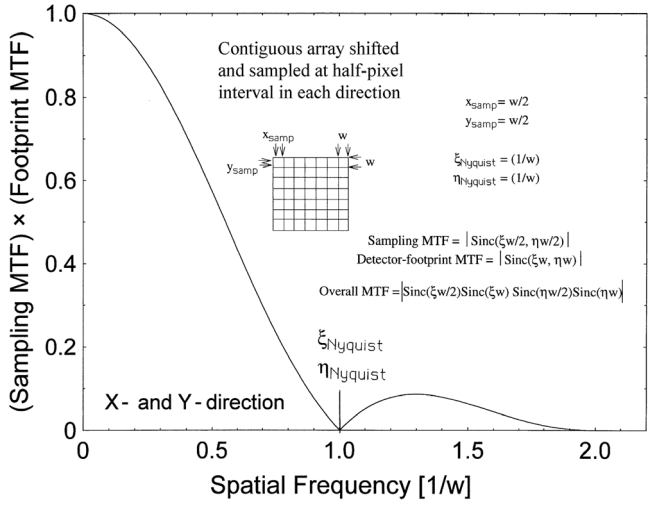

Figure 2.19 MTF for a contiguous focal-plane array with samples at half-pixel intervals in *x* and *y* directions.

Now we explore analogous sampling situations with a linear array of scanned detectors. The effective scan velocity relates temporal and spatial variables, and similarly relates temporal and spatial frequencies. Given a single detector scanned in the horizontal direction, the instantaneous field of view (IFOV) is that portion of the object scene being looked at by the detector at one instant in time. The IFOV is the moving footprint of the detector, and it has (spatial) dimensions of distance. As seen in Fig. 2.20, when the IFOV scans across a localized (delta function) feature in the scene, there will be a signal on the detector for a time period called the dwell time $\tau_d = \text{IFOV}/v_{\text{scan}}$ while the IFOV continuously moves across this feature.

We are free to decide the sampling interval for the time-domain analog waveform arising from a continuously scanned detector. Given $\tau_d = \text{IFOV}/v_{\text{scan}}$, the waveform sample spacings in time are directly related to spatial samplings in the scene's spatial variable x by $\Delta t = \Delta x/v_{\text{scan}}$. Thus, temporal frequencies and spatial frequencies are related by

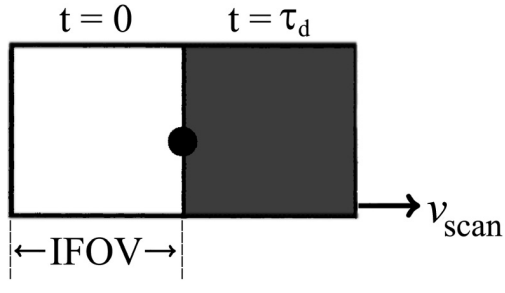

Figure 2.20 Two positions of a detector: at the start and at the end of the overlapping of the IFOV with a delta function scene feature.

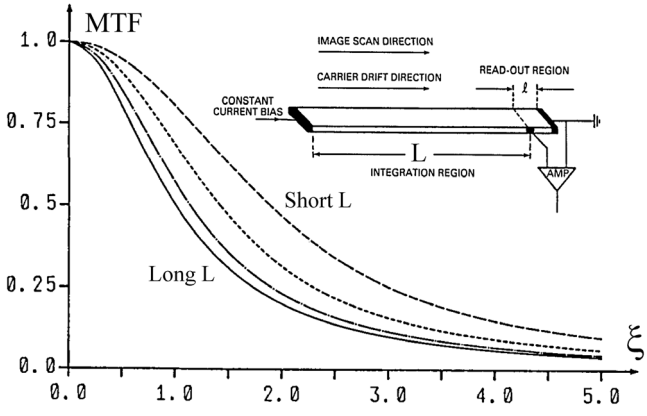

Fig. 2.29 MTF *vs* integration length for a SPRITE detector (adapted from Ref. 18).

an effective scan velocity v_{scan} in either image-plane spatial frequency or object-space angular spatial frequency:

$$f\,[\text{Hz}] = v_{\text{scan, image-plane}}\,[\text{mm/s}] \times \xi\,[\text{cy/mm}] \tag{2.18}$$

or

$$f\,[\text{Hz}] = v_{\text{scan, angular}}\,[\text{mrad/s}] \times \xi\,[\text{cy/mrad}]. \tag{2.19}$$

We can easily visualize the meaning of scan velocity for a scanned-sensor system such as that seen in Fig. 2.1 because the IFOV is actually moving across the object plane. It is not as easy to visualize scan velocity for a staring system like that seen in Fig. 2.2 because there is no motion of the IFOV. However, we can calculate a quantity having units of scan velocity if we know the field of view and the frame rate. In practice, it is not necessary to explicitly calculate the scan velocity to convert from temporal to spatial frequencies. We can determine the multiplicative factor experimentally using an electronic spectrum analyzer as seen in Fig. 2.30. First, we set up a bar target of known fundamental frequency that will create an image-plane spatial frequency which we can calculate (knowing the optical magnification) or which we can measure directly from the output signal (knowing the pixel-to-pixel spacing of the detector array). Taking the output video signal from the detector array into the spectrum analyzer will give us a readout of the electrical frequency corresponding to the fundamental image-plane spatial frequency of the bar target.

The transfer function of an electronic network can be tailored in ways that the transfer function of an optical system cannot. We can implement a boost filter that preferentially amplifies a particular band of frequencies, which can help to compensate for losses in modulation depth incurred in the optical

Chapter 3
Point-, Line-, and Edge-Spread Function Measurement of MTF

There are several ways we can measure MTF using targets that have an impulsive nature, each with positive aspects as well as drawbacks. In this chapter, we first develop the mathematical relationships between the data and the MTF for the point-spread function (PSF), line-spread function (LSF), and edge-spread function (ESF). One item of notation in this section is that we use * to denote a one-dimensional convolution, and ** to denote a two-dimensional convolution. We then compare the measurement techniques and consider options for increasing the signal-to-noise ratio and extending the spatial-frequency range of the measurements.

3.1 Point-Spread Function (PSF)

In the idealized arrangement of Fig. 3.1, we use a point source, represented mathematically by a two-dimensional delta function, as the object:

$$f(x, y) = \delta(x, y). \tag{3.1}$$

We initially assume that the image receiver is continuously sampled; that is, we do not need to consider the finite size of pixels nor the finite distance between samples. We will address these aspects of the measurement-instrument response later in this chapter. Here we assume that we can measure the image-irradiance distribution $g(x,y)$ to the necessary spatial precision. If the object is truly a point source, the two-dimensional image-irradiance distribution $g(x,y)$ equals the impulse response $h(x,y)$. This is also called the point-spread function (PSF):

$$g(x, y) = h(x, y) \equiv \mathrm{PSF}(x, y). \tag{3.2}$$

The PSF can be Fourier transformed in two dimensions to yield the two-dimensional OTF. Taking the magnitude yields the MTF:

use blackbodies as the flux sources. Having sufficient flux is usually not an issue in the visible because hotter sources are typically used.

The LSF method provides more image-plane flux than does the PSF test. The ESF setup provides even more flux and has the added advantage that a knife edge avoids slit-width issues. However, the ESF method requires a spatial-derivative operation, which accentuates noise in the data. If we reduce noise by convolution with a spatial kernel, the data-smoothing operation itself has an MTF contribution.

In any wavelength region, we can use a laser source to illuminate the pinhole. The spatial coherence properties of the laser do not complicate the interpretation of PSF data if the pinhole is small enough to act as a point source (by definition, spatially coherent regardless of the coherence of the illumination source). An illuminated pinhole acts as a point source if it is smaller than both the central lobe of the PSF of the system that illuminates the pinhole and the central lobe of the PSF of the system under test, geometrically projected (with appropriate magnification) to the source plane. Even with a laser-illuminated pinhole, the PSF measurement yields an incoherent MTF because the irradiance of the PSF is measured rather than the electric field.

For sources of extended spatial dimension, such as those for LSF and ESF tests, we must ensure that the coherence properties of the illumination do not introduce interference-fringe artifacts into the data.

3.5 Increasing SNR in PSF, LSF, and ESF Tests

We can use a variety of image-averaging techniques to increase the signal-to-noise ratio (SNR) in PSF, LSF, and ESF tests. These averaging techniques can be implemented in either the object plane or the image plane, provided we take steps to ensure that the data are the same in one direction and we average over that direction. We usually configure the illumination level in the measurement apparatus such that the shot noise of the signal dominates the noise in the measurement. This means that the root-mean-square (rms) noise grows in proportion to the square root of the signal. In this case, the SNR increases in proportion to the square root of the signal level. In an averaging procedure, the signal is proportional to the number of independent samples. Therefore, we can achieve a considerable SNR advantage if we average a large number of samples (such as the rows in a typical CCD array). In certain instances (such as operation in the amplifier-noise limit or another signal-independent noise floor), the SNR can grow as fast as linearly with respect to the number of samples.

3.5.1 Object- and image-plane equivalence

This technique requires that we assume that we match the object and receiver symmetry for optimum flux collection. We equate higher flux collection to

Chapter 4
Square-Wave and Bar-Target Measurement of MTF

Although MTF is defined in terms of the response of a system to sinusoids of irradiance, we commonly use binary targets in practice because sinusoidal targets require analog gray-level transmittance or reflectance. Fabricating targets with analog transmittance or reflectance usually involves photographic or lithographic processes with spatial resolutions much smaller than the period of the sinusoid so that we can achieve an area-averaged reflectance or transmittance. Sinusoidal targets used in MTF testing should have minimal harmonic distortion so that they present a single spatial frequency to the system under test. This is difficult to achieve in the fabrication processes. Conversely, binary targets of either 1 or 0 transmittance or reflectance are relatively easy to fabricate. We can fabricate binary targets for low spatial frequencies by machining processes. For targets of higher spatial frequency, we can use optical-lithography processes of modest resolution because the metallic films required to produce the binary patterns are continuous on a micro scale. In this chapter, we will first consider square-wave targets and then three-bar and four-bar targets. Square-wave targets not only consist of the fundamental spatial frequency, but also contain higher harmonic terms. Bar targets contain both higher and lower harmonics of the fundamental. Because of these harmonics, we must correct modulation-depth measurements made with binary targets to produce MTF data, either with a series approach or with digital filtering.

4.1 Square-Wave Targets

Targets that have an infinite number of square-wave cycles are simple to analyze mathematically. Figure 4.1 shows a portion of an infinite square wave (equal lines and spaces) and its spectrum. The spectrum consists of a series of delta functions at dc, the fundamental frequency (the inverse of bar spacing), and third, fifth, and higher odd harmonics. The one-sided amplitude of the

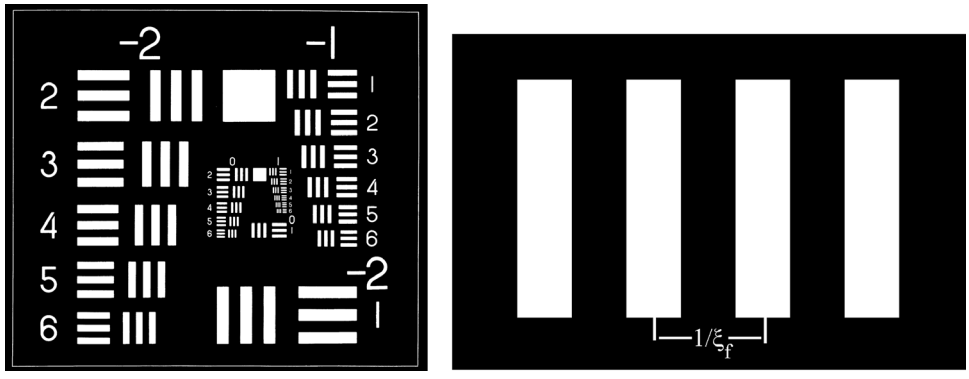

Figure 4.3 Binary (left) three-bar and (right) four-bar transmission targets.

remove these non-fundamental-frequency components by computation, or we filter them out electronically or digitally to yield MTF data.

We determine the modulation depth of the output image from the maximum and minimum values of the irradiance waveform of the three- or four-bar target. Often the effects of aberrations, shading, or aliasing produce maxima and minima that are not equal for each bar in the output image, as seen in Fig. 4.4. We calculate the modulation depth using the highest peak (maximum) of one or more of the bars and the lowest inter-bar minimum to occur in any particular image.

As a practical note, if we are measuring the modulation depth of a bar target and cannot adjust the fine positional alignment of the target so that all four bars have the same height at the output, then we are probably trying to measure MTF at too high a frequency. The measurement accuracy of the

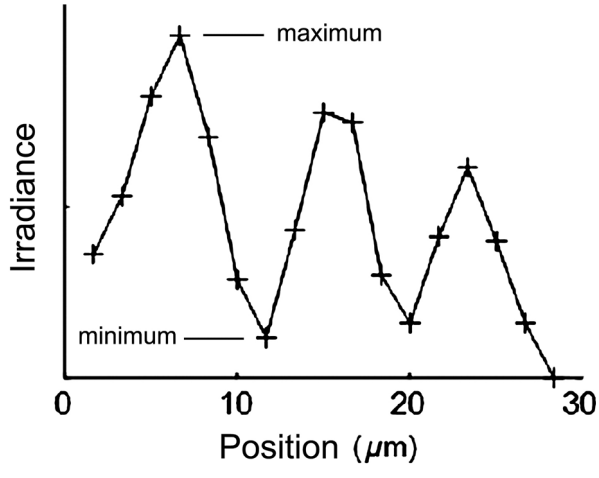

Figure 4.4 Measurement of three-bar IMD from unequal bar data (adapted from Ref. 4).

Chapter 5
Noise-Target Measurement of MTF

Measurement of a system's transfer function by means of its response to random-noise inputs has long been a standard procedure in time-domain systems.[1] If the input is white noise, which contains equal amounts of all frequencies, the action of the transfer function is to impart a nonuniformity of frequency content that can be assessed at the output of the system by means of a Fourier analysis. This concept has not historically been employed in the measurement of optical systems, with the exception of an initial demonstration[2] using (non-white) film-grain noise.

Noise-like targets of known spatial-frequency content are useful for MTF testing, particularly for spatially sampled systems such as detector-array image receivers. Noise targets have a random position of the image data with respect to sampling sites in the detector array and measure a shift-invariant MTF that inherently includes the sampling MTF. Noise targets measure the MTF according to

$$\mathrm{PSD}_{\mathrm{output}}(\xi, \eta) = \mathrm{PSD}_{\mathrm{input}}(\xi, \eta) \times [\mathrm{MTF}(\xi, \eta)]^2, \tag{5.1}$$

where PSD denotes power spectral density, defined as the ensemble average of the square of the Fourier transform of object or image data. The PSD is a measure of spatial-frequency content for random targets or random images. We calculate the output PSD from the image data. Generally, we calculate the finite-length Fourier transform of a row of image data and square the result. This is an estimate of the PSD, but because the calculation is performed on a data record of finite length, there is noise in the estimate. When we perform this operation on other rows of image data, we generate other PSD estimates. Averaging over these additional estimates gives a more accurate estimation[3] of the PSD of the underlying random process. Noise targets usually measure the MTF averaged over a system's whole field of view. However, we can calculate PSDs from various subregions of the image. If we use smaller data

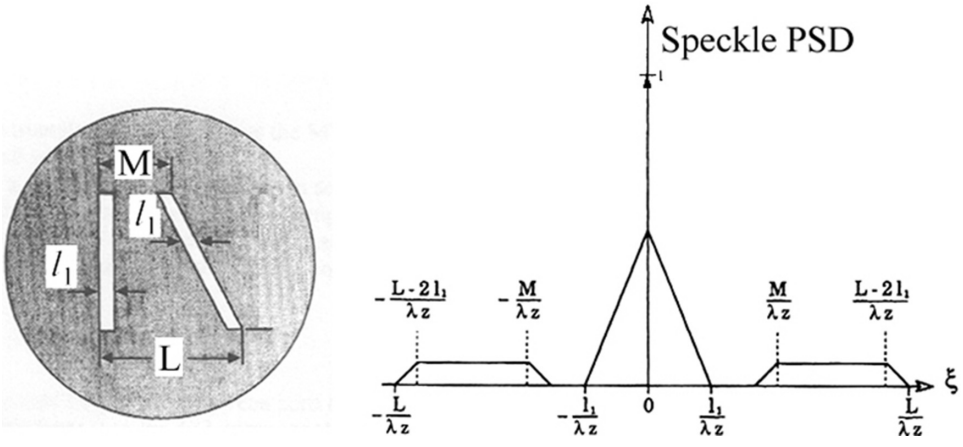

Figure 5.7 (left) Slanted-dual-slit aperture and (right) its ξ-direction PSD (reprinted from Ref. 10).

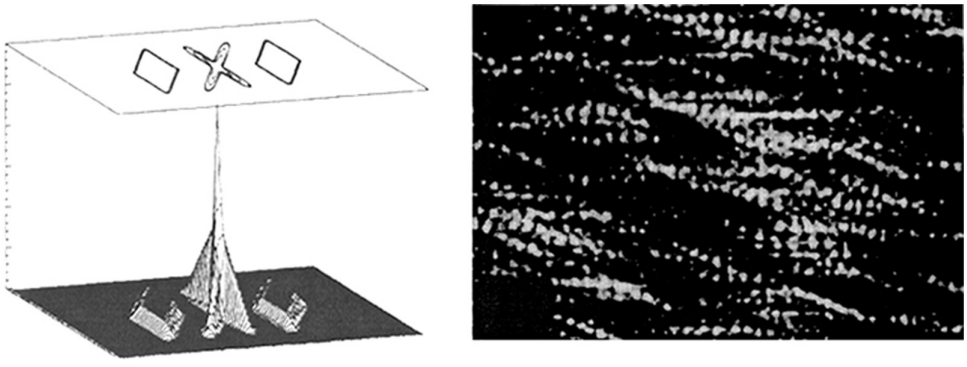

Figure 5.8 (left) Two-dimensional PSD plot and (right) a speckle pattern from the slanted-dual-slit aperture of Fig. 5.7 (reprinted from Ref. 10).

Figure 5.9 shows another two-dimensional aperture[11] that generates a constant input PSD over an extended frequency range along the ξ direction. An autocorrelation of the aperture in the x direction produces the PSD form as shown. Figure 5.10 shows a plot of the two-dimensional PSD and a speckle pattern resulting from this aperture. This configuration has been used for measurement of detector array MTF beyond the Nyquist frequency in the following manner. A measurement of MTF out to Nyquist was first performed using the flat region of the PSD. The aperture-to-detector distance was then decreased so that the flat region of the PSD ranged from Nyquist to twice Nyquist. A new output PSD was acquired, which aliased the high-frequency information onto the original un-aliased PSD. A PSD subtraction was performed, which yielded only the high-frequency PSD. The un-aliased PSD and the high-frequency PSD were then concatenated, and Eq. (5.1) was

Chapter 6
Practical Measurement Issues

In this chapter, we will consider a variety of practical issues related to MTF measurement, including the cascade property of MTF multiplication, the quality of the auxiliary optics such as collimators and relay lenses, source coherence, and normalization at low frequency. We will conclude with some comments about the repeatability and accuracy of MTF measurements and the use of computers for data acquisition and processing. At the end of the chapter, we will consider four different instrument approaches that are representative of commercial MTF equipment and identify the design tradeoffs.

6.1 Measurement of PSF

We begin with a useful approximate formula. For a uniformly distributed blur spot of full width w, the resulting MTF, shown in Fig. 6.1, is

$$\mathrm{MTF}(\xi) = \left| \frac{\sin(\pi \xi w)}{(\pi \xi w)} \right|. \tag{6.1}$$

We can use this simple approach as a handy reality check, comparing a measured spot size to computer-calculated MTF values. Often when computers are part of the data-acquisition and data-processing procedures, we cannot check and verify each step of the MTF calculation. In these situations, it is a good idea to manually verify the results of the computation by using a measuring microscope to assess the size of the impulse response formed by the system.

Figure 6.2 shows a convenient configuration[1] for a visible-band PSF measurement that is easy to assemble. A microscope objective is paired with a Si charge-coupled-device (CCD) camera head by means of threaded adapter rings. Even if the distance between the objective and the CCD image plane is not the standard 160 mm for a microscope, an in-focus image will be formed when the impulse response being viewed is at some small distance in front of the objective. It is convenient to use a ground-glass screen on which to project

Chapter 7
Other MTF Contributions

We now consider the MTF contributions arising from image motion, image vibration, atmospheric turbulence, and aerosol scattering. We present a first-order analysis of these additional contributions to the system MTF. Our heuristic approach provides a back-of-the-envelope estimate for the image-quality impact of these effects, and a starting point for more advanced analyses.

7.1 Motion MTF

Image-quality degradation arises from movement of the object, image receiver, or optical-system line of sight during an exposure time τ_e. We consider uniform linear motion of the object at velocity v_{obj} and a corresponding linear motion of the image at velocity v_{img}, as shown in Fig. 7.1. Over an exposure time τ_e, the image has moved a distance $v_{img} \times \tau_e$. This one-dimensional motion blur can be modeled as a rect function:

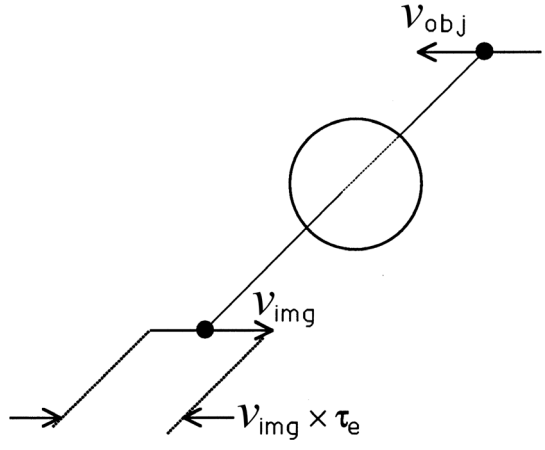

Figure 7.1 Linear motion blur is the product of image velocity and exposure time.

analysis to predict the number of exposures required to get a single lucky shot where there is no more than a prescribed degree of motion blur.[2]

7.3 Turbulence MTF

Atmospheric turbulence results in image degradation. We consider a random phase screen (Fig. 7.5) with an autocorrelation width w that is the size of the refractive-index eddy and a phase variance σ^2. The simplest model is one of cloud-like motion, where the phase screen moves with time but does not change form—the frozen-turbulence assumption. We model an average image-quality degradation over exposure times that are long compared with the motion of the phase screen. Image quality estimates for short exposure times require more complicated models.

We consider diffraction from the eddys to be the cause of MTF degradation (blurring). We assume that $w \gg \lambda$, which is consistent with the typical eddy sizes (1 cm $< w <$ 1 m) encountered in practice. Refractive ray-deviation errors can be determined from a separate angle-of-arrival analysis, resulting in image-plane motion (distortion). As seen in Fig. 7.6, the impulse response $h(x)$ consists of a narrow central core from the unscattered radiation and a wide diffuse region from the scattered radiation. Larger phase variation in the screen leads to more of the impulse-response power being contained in the scattered component.

The narrow central core of the impulse response contributes to a broad flat MTF at high frequencies. The broad diffuse scattered component of the impulse response will contribute to an MTF rolloff at low frequencies. We can write[3] the turbulence MTF as

$$\mathrm{MTF}(\xi) = \exp\left\{-\sigma^2\left[1 - \exp\left\{-\left(\frac{\lambda\xi}{w}\right)^2\right\}\right]\right\}, \tag{7.3}$$

where ξ is the angular spatial frequency in cycles/radian. This MTF is plotted in Fig. 7.7, with the phase variance as a parameter. For a phase variance near zero, turbulence contributes minimal image-quality degradation because most

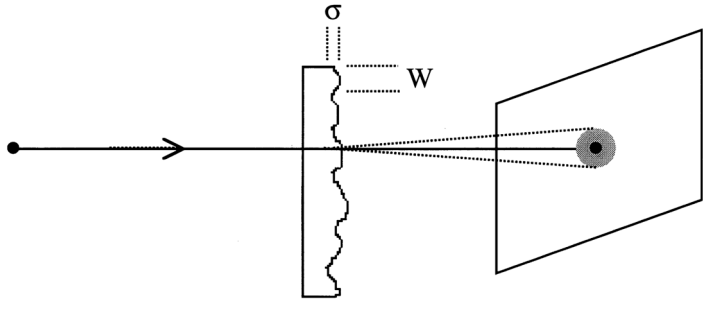

Figure 7.5 Frozen-turbulence model for a phase screen.

Glenn D. Boreman is Professor and Chairman of the Department of Physics & Optical Science and Director of the Center for Optoelectronics & Optical Communications at the University of North Carolina at Charlotte. He is co-founder and Board Chairman of Plasmonics, Inc. (Orlando). From 1984 to 2011 he was on the faculty of the University of Central Florida, where he is now Professor Emeritus. He has supervised to completion 35 MS and 27 PhD students. He has held visiting research positions at IT&T (Roanoke), Texas Instruments (Dallas), US Army Night Vision Lab (Ft. Belvoir), McDonnell Douglas Astronautics (Titusville), US Army Redstone Arsenal (Huntsville), Imperial College (London), Universidad Complutense (Madrid), Swiss Federal Institute of Technology (Zürich), Swedish Defense Research Agency (Linköping), and University of New Mexico (Albuquerque). He received the BS in Optics from the University of Rochester, and the PhD in Optics from the University of Arizona. Prof. Boreman served as Editor-in-Chief of *Applied Optics* from 2000 to 2005, and Deputy Editor of *Optics Express* from 2014 to 2019. He is coauthor of the graduate textbooks *Infrared Detectors and Systems* and *Infrared Antennas and Resonant Structures* (SPIE Press), and author of *Modulation Transfer Function in Optical & Electro-Optical Systems* (SPIE Press) and *Basic Electro-Optics for Electrical Engineers* (SPIE Press). He has published more than 200 refereed journal articles in the areas of infrared sensors and materials, optics of random media, and image-quality assessment. He is a fellow of SPIE, IEEE, OSA, and the Military Sensing Symposium. He is a Professional Engineer registered in Florida. Prof. Boreman served as the 2017 President of SPIE.